Analysis and Tracking of Optimal Load in Wireless Power Transfer Systems

Minfan Fu, *Student Member, IEEE*, He Yin, *Student Member, IEEE*, Xinen Zhu, *Member, IEEE*, and Chengbin Ma, *Member, IEEE*

***Abstract*—All the wireless power transfer (WPT) systems share a similar configuration including a power source, a coupling system, a rectifying circuit, a power regulating, and charging management circuit and a load. For such a system, both a circuit- and a system-level analyses are important to derive requirements for a high overall system efficiency. Besides, unavoidable uncertainties in a real WPT system require a feedback mechanism to improve the robustness of the performance. Based on the above basic considerations, this paper first provides a detailed analysis on the efficiency of a WPT system at both circuit and system levels. Under a specific mutual inductance between the emitting and receiving coils, an optimal load resistance is shown to exist for a maximum overall system efficiency. Then, a perturbation-and-observation-based tracking system is developed through additional hardware such as a cascaded boost-buck dc–dc converter, an efficiency sensing system, and a controller. Finally, a 13.56-MHz WPT system is demonstrated experimentally to validate the efficiency analysis and the tracking of the optimal load resistances. At a power level of 40 W, the overall efficiency from the power source to the final load is maintained about 70% under various load resistances and relative positions of coils.**

***Index Terms*—Efficiency analysis, inductive resonance coupling, tracking of optimum load resistance, wireless power transfer.**

I. Introduction

MAXWELL's equations explain how electric and magnetic fields are generated and altered by each other. The equations form a foundation of today's wireless communication technologies. Compared to the signal energy in communication, a much large amount of energy can be propagated in space actually based on a same physics, i.e., the wireless power transfer (WPT). The eletrophysicist, Nikola Tesla, first proposed this idea of WPT in 1904 in order to build a "world system" for "transmission of electrical energy without wires" [1]. Early experimental attempts failed due to the limitations of technology at that time. In recent years, due to a dramatic need in charging of various electronic devices (e.g., cellphones, laptop computers, tablets, medical implant devices, etc.), there is a strong interest renewed in the research and applications of the WPT technologies. It is desired by users to have a ubiquitous access to both information and electrical power through air. For the devices and systems that require large power, such as robots and electric vehicles, WPT not only provides a convenient and safe noncontacting charging, but also opens a new direction in on-board energy and power management. Currently, batteries are one of the most popular mobile power sources. However, there are several challenges for batteries to be addressed, such as limited energy and power densities, slow charging rate, reliability, weight, and cost. It is significant that WPT provides a viable solution without the need of dramatic improvements in battery technology [2], [3].

There are multiple technological options for WPT, such as inductive coupling, magnetic coupling, microwave, and laser radiation. They have various power level, working frequency, transfer distance, size and forming factors that are preferred by a certain specific application over the others. Using far field, microwave and laser radiation can transfer power over meters or hundreds of meters, but the power level is relatively small in order to avoid hazardous radiation [4], [5]. In addition, a large size antenna array is usually required to focus the radiation beam. On the contrary, the inductive coupling and magnetic resonance coupling use near field. The transfer distance is usually limited to a range of centimeters, while the transferred power can reach a level of tens of kilowatts. In the magnetic resonance coupling systems, the emitting and receiving coils are designed to have a same natural frequency, i.e., resonant inductive coupling. Since the magnetic coupling systems usually work in megahertz band, the inherent capacitances of the coils are used [6]. The inductive coupling systems working in kilohertz band (such as at 20 KHz) are also usually tuned to resonance but using external capacitors [7], [8]. Mostly due to the availability of the state-of-art power electronic devices operating at kilohertz, the inductive coupling systems are widely used in both low and high power applications [9]–[12]. On the other hand, for a more compact and lighter WPT system, higher frequency, such as megahertz, is usually desired. However, there are limitations in the performance of today's power electronic devices, the usable frequency range under the regulation of ISM (industrial, scientific, and educational) band, etc. [13], [14]. Current studies mainly deal with low power WPT systems working in megahertz band [15].

Despite various technologies, all the WPT systems share a similar configuration including a power source, a coupling system, a rectifying circuit, a power regulating, and charging management circuit (such as a dc–dc converter) and a load (see

Manuscript received April 7, 2014; revised June 26, 2014; accepted July 29, 2014. Date of publication August 12, 2014; date of current version February 13, 2015. This work was supported by National Science Foundation of China under Grant 50950110341(2010) and Grant 61102019(2012-2014). Recommended for publication by Associate Editor C. T. Rim.

M. Fu, H. Yin, and X. Zhu are with the University of Michigan-Shanghai Jiao Tong University Joint Institute, Shanghai Jiao Tong University, Minhang, Shanghai 200240, China (e-mail: fuminfan@sjtu.edu.cn; yyy@sjtu.edu.cn; zhuxinen@sjtu.edu.cn).

C. Ma is with the University of Michigan-Shanghai Jiao Tong University Joint Institute, Shanghai Jiao Tong University, Minhang, Shanghai 200240, China; and also with School of Mechanical Engineering, Shanghai Jiao Tong University, Shanghai 201101, China (e-mail: chbma@sjtu.edu.cn).

Color versions of one or more of the figures in this paper are available online at http://ieeexplore.ieee.org.

Digital Object Identifier 10.1109/TPEL.2014.2347071

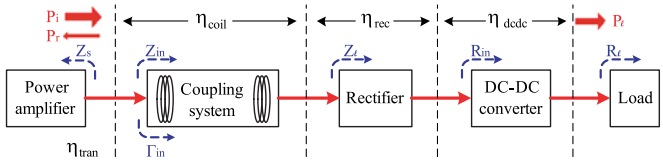

Fig. 1. System configuration.

Fig. 1). For such a system, besides an optimized design of each circuit, a system-level analysis is important to derive requirements for a high overall efficiency [16]–[22]. In real environments, there are unavoidable uncertainties in a WPT system such as the variations in relative position of coils, load characteristics, etc. A feedback mechanism is necessary to improve the robustness of the performance of the WPT system. Most of existing methods discuss the efficiency improvement when the relative position varies between the emitting and receiving coils. The tracking of the resonance frequency is widely used in kilohertz WPT systems [23]. A similar method can also be applied in megahertz systems. However, the existing ISM band is usually too narrow to accommodate the frequency tracking [14], [24]. A variable coupling method was proposed for a WPT system using four symmetric coils [25]. A high efficiency is achieved by adjusting the coupling factor (i.e., distance) between the source (load) and the internal coils in the case of coil distance variations. A tunable impedance matching before the coupling coils was studied in order to reduce the reflected power due to a varying coil distance [26]. Based on the detected ratio of the reflected power, the parameters of the network are adjusted by controlling multiple relays to switch among different combinations of capacitors and inductors.

Though impedance matching is a straightforward method to overcome power reflection, the network itself may introduce additional power loss due to unavoidable nonideal capacitors and inductors, as well as an increased system complexity. It is also difficult to design an impedance matching network when the load is changing over time. A static control of a novel cascaded boost-buck dc–dc converter was proposed to provide an optimal equivalent load resistance, and thus a high overall system efficiency for various loads such as resistive loads, ultracapacitors, and batteries [27]. The dc–dc converter not only minimizes the effect of a dynamic load to the system efficiency, but also alleviates the requirements for impedance matching networks. In this paper, the interactive relationships among the efficiencies of each circuit and the overall WPT system, mutual inductance, and load resistance are further analyzed in order to provide a guideline for the design of a feedback-based dynamic control. Particularly, here the overall efficiency of the WPT system is defined as the ratio of the power received by the final load to the incident power from the power source. It is found that an optimal load resistance exists under a specific mutual inductance, i.e., a certain relative position of coils. The tracking of the optimal load resistances is then proposed and implemented in a final experimental system. Through the tracking control, a high overall system efficiency can be maintained when variations occur in relative position of coils (such as distance) and load characteristics.

This paper is organized as follows. In Section II a detailed investigation into efficiencies in an example WPT system is carried out. The efficiencies include the efficiencies of each circuits and the overall system efficiency. Then, the requirement on an optimal load resistance is derived and explained based on the interactive relationships among the efficiencies, the mutual inductance of coils, and the load resistance. In Section III the tracking of the optimal load resistances is discussed, which applies a perturbation and observation (P&O)-based algorithm. For the implementation of the tracking control, the cascaded dc–dc converter, an efficiency sensing system, and a National Instrument (NI) CompactRIO-based controller are integrated in the final experimental WPT system. Then in Section IV the theoretical analysis and tracking system design are validated by experimental results. Finally, the conclusion is drawn in Section V.

II. System Efficiency Analysis

A. Definition of Efficiency

Fig. 1 shows the configuration of the WPT system discussed in this paper. The system is a 13.56-MHz medium power WPT system (40 W). It includes a power amplifier (PA), a coupling system, a rectifier, a dc–dc converter, and a load. As shown in the figure, $Z_{\rm in}$ and Z_l are defined as the impedances seen by the PA and the coupling system, respectively. $R_{\rm in}$ is the load resistance seen by the rectifier. R_l is the final load. $\Gamma_{\rm in}$ is the reflection coefficient of the PA [28]. Here, the system efficiency $\eta_{\rm sys}$ is defined as

$$\eta_{\rm sys} = \frac{P_l}{P_i} \tag{1}$$

where P_l is the power received by the final load, and P_i is the incident power from the PA. Note the PA efficiency is not included in this definition. As mentioned in Section I the focus here is on the general discussion on the loading effect and control in megahertz WPT systems. The following study and findings could be applicable to many PA topologies for WPT application.

The system efficiency defined here can also be represented as

$$\eta_{\rm sys} = \eta_{\rm tran} \cdot \eta_{\rm coil} \cdot \eta_{\rm rec} \cdot \eta_{\rm dcdc} \tag{2}$$

where $\eta_{\rm coil}$, $\eta_{\rm rec}$, and $\eta_{\rm dcdc}$ are the efficiencies of the coupling system, the rectifier, and the dc–dc converter, respectively. The efficiency $\eta_{\rm tran}$ describes the power reflection between the PA and the following subsystems, i.e.,

$$\eta_{\rm tran} = \frac{P_i - P_r}{P_i} \tag{3}$$

where P_r is the reflected power to the PA.

B. Simplified Circuit Model

Fig. 2 shows the equivalent circuit model of the simplified WPT system. In the model, Z_s represents the source impedance of the PA. Z_s is usually designed to match a standard impedance such as 50 Ω for radio frequency (RF) power sources. Z_l is the equivalent impedance of the following subsystems after the coupling system [see Fig. 1]. The coupling system is described

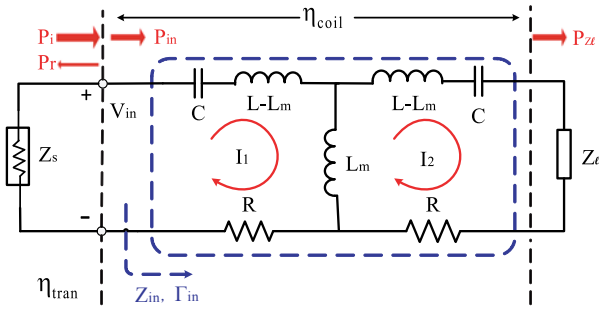

Fig. 2. Equivalent circuit model of the simplified WPT system.

by a series resistor–inductor–capacitor (RLC) circuit model. The magnetic coupling is modeled by the mutual inductance L_m. Here, $L_m = k \cdot L$, where k is the mutual-inductance coefficient.

Based on the circuit model in Fig. 2, the following relationships can be derived:

$$I_1\left(R+\frac{1}{j\omega C}+j\omega L\right)-I_2 j\omega L_m - V_{\text{in}} = 0 \tag{4}$$

$$I_2\left(Z_l+R+\frac{1}{j\omega C}+j\omega L\right)-I_1 j\omega L_m = 0. \tag{5}$$

Therefore,

$$I_1 = \frac{(Z_l+R+\frac{1}{j\omega C}+j\omega L)V_{\text{in}}}{(R+\frac{1}{j\omega C}+j\omega L)(Z_l+R+\frac{1}{j\omega C}+j\omega L)+\omega^2 L_m^2} \tag{6}$$

$$I_2 = \frac{j\omega L_m V_{\text{in}}}{(R+\frac{1}{j\omega C}+j\omega L)(Z_l+R+\frac{1}{j\omega C}+j\omega L)+\omega^2 L_m^2} \tag{7}$$

and the input impedance Z_{in}, the load of the PA, is

$$Z_{\text{in}} = \frac{V_{\text{in}}}{I_1}. \tag{8}$$

Then, the efficiency η_{tran} can be calculated as

$$\eta_{\text{tran}} = \frac{P_i - P_r}{P_i} = \frac{P_{\text{in}}}{P_i} = 1 - |\Gamma_{\text{in}}|^2 \tag{9}$$

where P_{in} is the power received by the coupling system, and Γ_{in} is the reflection coefficient

$$\Gamma_{\text{in}} = \frac{Z_{\text{in}} - Z_s}{Z_{\text{in}} + Z_s}. \tag{10}$$

If resonance occurs, i.e., $j\omega L + \frac{1}{j\omega C} = 0$, the calculation of Z_{in} can be further simplified as

$$Z_{\text{in}} = R + \frac{\omega^2 L_m^2}{Z_l + R} \tag{11}$$

and η_{tran} becomes

$$\eta_{\text{tran}} = \frac{4Z_s(R+Z_l)(R^2+RZ_l+\omega^2 L_m^2)}{[(R+Z_s)(R+Z_l)+\omega^2 L_m^2]^2}. \tag{12}$$

In order to eliminate the power reflection, conjugate matching should be satisfied, namely $Z_{\text{in}} = Z_S^*$. Using (11), the Z_l for zero power reflection, $Z_{l,\text{tran,opt}}$, can be derived as

$$Z_{l,\text{tran,opt}} = \frac{\omega^2 L_m^2}{Z_S^* - R} - R. \tag{13}$$

Here, the efficiency for the coupling system, η_{coil}, is defined as

$$\eta_{\text{coil}} = \frac{P_{Z_l}}{P_{\text{in}}} \tag{14}$$

where P_{Z_l} is the power received by the load Z_l, the impedance seen by the coupling system. Thus, under the resonance

$$\eta_{\text{coil}} = \frac{|I_2|^2 Z_l}{I_1 V_{\text{in}}} = \frac{\omega^2 L_m^2 Z_l}{(R^2+RZ_l+\omega^2 L_m^2)(Z_l+R)}. \tag{15}$$

The optimal Z_l, $Z_{l,\text{coil,opt}}$, for a maximum η_{coil} can be calculated by taking the first-order derivative

$$Z_{l,\text{coil,opt}} = \sqrt{R^2+\omega^2 L_m^2}. \tag{16}$$

Similarly, the system efficiency is

$$\eta'_{\text{sys}} = \frac{P_{Z_l}}{P_i} = \eta_{\text{tran}} \cdot \eta_{\text{coil}} = \frac{4Z_l Z_s \omega^2 L_m^2}{[(R+Z_s)(R+Z_l)+\omega^2 L_m^2]^2} \tag{17}$$

and its corresponding optimal Z_l is

$$Z_{l,\text{opt}} = R + \frac{\omega^2 L_m^2}{R+Z_s}. \tag{18}$$

TABLE I
PARAMETERS OF THE TWO RESONANCE COILS

Resonant frequency	13.56 MHz
Self-inductance L	7.8 μH
Self-capacitance C	17.6 pF
Parasitic resistance R	3.4 Ω

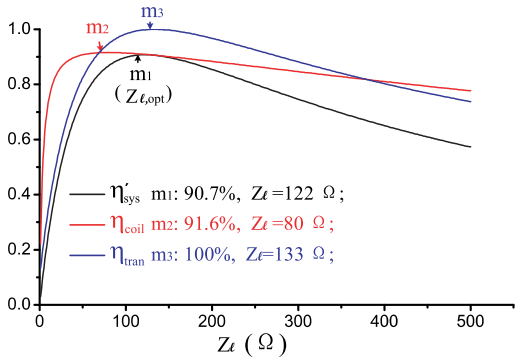

Fig. 3. Comparison on efficiencies versus Z_l when $k = 0.12$.

Table I lists the parameters of resonance coils measured by vector network analyzer (VNA) from a real coupling system used in the final experiment [see Section III-C]. The efficiencies versus Z_l under a constant k (=0.12), η_{tran}, η_{coil}, and η'_{sys}, are shown in Fig. 3. Three points m_1, m_2, and m_3 are labeled to show an optimal Z_l for each efficiency. $Z_{l,\text{opt}}$ is the optimal Z_l for a maximum η'_{sys}. It can be seen that the optimal Z_ls for the

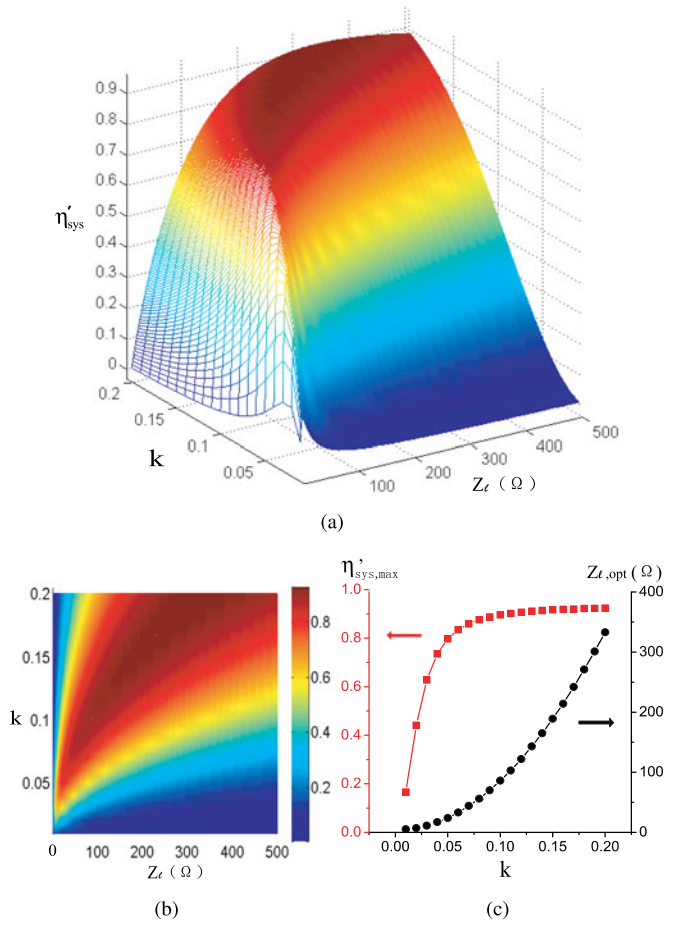

Fig. 4. $\eta'_{\rm sys}$ under different Z_l and k. (a) 3-D view. (b) 2-D view. (c) Optimal Z_l's ($Z_{l,\rm opt}$).

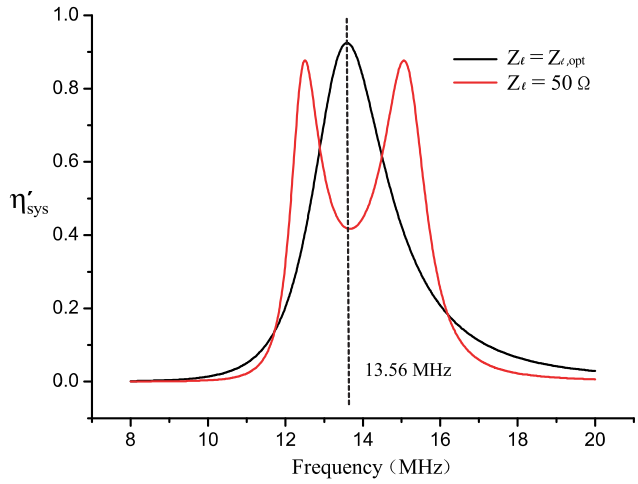

Fig. 5. Efficiency comparisons for $Z_l = Z_{l,\rm opt}$ and $Z_l = 50\ \Omega$ when $k = 0.2$.

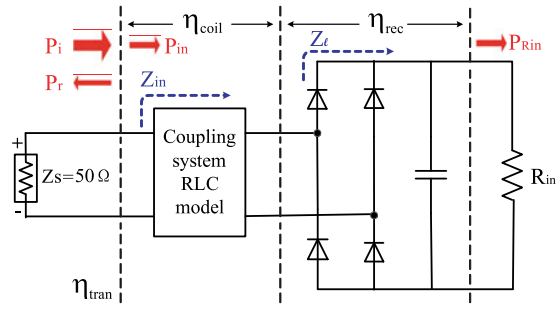

Fig. 6. System configuration with a rectifier.

efficiencies are different. A subsystem-level optimization, such as for $\eta_{\rm tran}$ or $\eta_{\rm coil}$, does not necessarily guarantee an optimal overall system. There are complicated interactive relationships among the subsystems and various uncertainties (such as variations in relative position of coils and load) in a real WPT system. System-level analysis and optimization are important.

$\eta'_{\rm sys}$ is further analyzed under various k and Z_l simulating uncertainties in relative position of coils and load, respectively. The results are shown in Fig. 4. The optimal load $Z_{l,\rm opt}$ versus k and its corresponding maximum $\eta'_{\rm sys}$ ($\eta'_{\rm sys,max}$) are summarized in Fig. 4(c). The figure shows that a high system efficiency can be maintained within a wide range of k, and the maximum efficiency $\eta'_{\rm sys,max}$ is increased when k is increased. As shown in Fig. 5, in the conventional S-parameter simulation, for a large k such as 0.2, the resonance frequency split is observed, and the system efficiency $\eta'_{\rm sys}$ at the targeted 13.56 MHz is reduced (red curve). This observation is explained by the constant 50 Ω load (Z_l), while under the optimal load $Z_{l,\rm opt}$, the maximum system frequency $\eta'_{\rm sys,max}$ is achieved (black curve). Therefore, in Fig. 4(c) $\eta'_{\rm sys,max}$ is actually increased with an increasing k. These results indicate that for a WPT system working in a dynamic environment, its overall efficiency can be improved by tracking the optimal load, i.e., $Z_{l,\rm opt}$ in Fig. 4(c).

C. System With Rectifier

In the above section, the impedance Z_l is the equivalent input impedance of the following subsystems, among which usually a rectifier is included. For a conventional full-bridge rectifier, as shown in Fig. 6, there exists an optimal $R_{\rm in}$, the load resistance seen by the rectifier, that maximizes the system efficiency. Similarly, the overall system efficiency $\eta''_{\rm sys}$ here is defined as

$$\eta''_{\rm sys} = \frac{P_{R_{\rm in}}}{P_i} = \eta_{\rm tran} \cdot \eta_{\rm coil} \cdot \eta_{\rm rec} \tag{19}$$

where $P_{R_{\rm in}}$ is the power received by the load $R_{\rm in}$. An optimal $R_{\rm in}$ ($R_{\rm in,opt}$) is determined in such a way that $\eta''_{\rm sys}$ is maximized. Due to the nonlinear nature of rectifiers and complex model of Schottky diodes, it is difficult to derive the exact analytical expression of $R_{\rm in,opt}$. Instead a nonlinear circuit simulation tool, the advanced design system (ADS) from Agilent, is used to evaluate the various efficiencies $\eta_{\rm tran}$, $\eta_{\rm coil}$, $\eta_{\rm rec}$, and $\eta''_{\rm sys}$. $\eta_{\rm rec}$ is the efficiency of the rectifier.

As discussed above, in megahertz WPT systems, the power reflection becomes much more obvious than that in kilohertz systems. This requires simulation software to be able to analyze the impedances at different ports. The conventional simulation software for power electronics can provide accurate circuit-level analysis in time domain. However, they are not suitable for

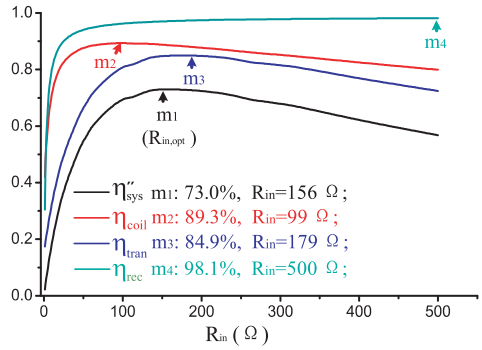

Fig. 7. Comparison on efficiencies by sweeping $R_{\rm in}$ when $k = 0.12$.

analyzing impedances in frequency domain. Here, the widely used RF software ADS is introduced in order to analyze the power reflection and the subsystem efficiencies. ADS can provide large-signal S-parameter (LSSP) simulation and harmonic balance (HB) simulation simultaneously. LSSP computes the S-parameters, gives the impedances at different ports, and evaluates $\eta_{\rm tran}$, while HB is a frequency-domain analysis tool for simulating distortion in nonlinear circuits and systems. HB can obtain voltages and currents in frequency domain, and thus directly calculate the steady-state spectral content of voltages or currents in megahertz WPT systems. Finally, the inputs and outputs at different ports are used to analyze the efficiencies such as $\eta_{\rm coil}$ and $\eta_{\rm rec}$. In the ADS-based simulation, the power source is a port of 40 W with 50-Ω source impedance. The rectifier circuit is built using the Pspice model of the SiC Schottky diodes (STPSC406 from STMicroelectronics, the diodes used in the final experimental system). The model is imported into ADS for the LSSP and HB simulation.

Fig. 7 shows the efficiencies versus $R_{\rm in}$ under a constant mutual-inductance coefficient k (=0.12). It can be seen that $\eta_{\rm rec}$ is almost constant over a wide range of $R_{\rm in}$ and $\eta''_{\rm sys}$ is now determined by the product of $\eta_{\rm tran}$, $\eta_{\rm coil}$, and $\eta_{\rm rec}$. Again, $\eta''_{\rm sys}$ is further analyzed under various k and $R_{\rm in}$. The results are shown in Fig. 8. The optimal load resistance $R_{\rm in,opt}$ versus k and its corresponding $\eta''_{\rm sys}$ are summarized in Fig. 8(c). Similarly, tracking of the optimal load resistances $R_{\rm in,opt}$s, can maintain a maximum system efficiency $\eta_{\rm sys,max''}$ under a specific k.

Meanwhile, it should be noticed that compared to $\eta'_{\rm sys}$ in Fig. 4(c), the maximum $\eta''_{\rm sys}$ in Fig. 8(c) is not monotonic anymore. With an increasing k, $\eta''_{\rm sys}$ first increases, and then starts to actually drop. This result seems to be against the usual experience that a stronger coupling of the coils leads to a higher system efficiency. It is because the discussion here focuses on the effect of the load $R_{\rm in}$. In order to further investigate this phenomenon, all the maximum efficiencies versus k are compared in Fig. 9, i.e., with their respective optimal $R_{\rm in}$s. It can be seen that

1) maximum $\eta_{\rm coil}$ increases with a larger k, which matches the usual experience;
2) maximum $\eta_{\rm rec}$ is almost constant, i.e., a limited influence on $\eta''_{\rm sys}$;

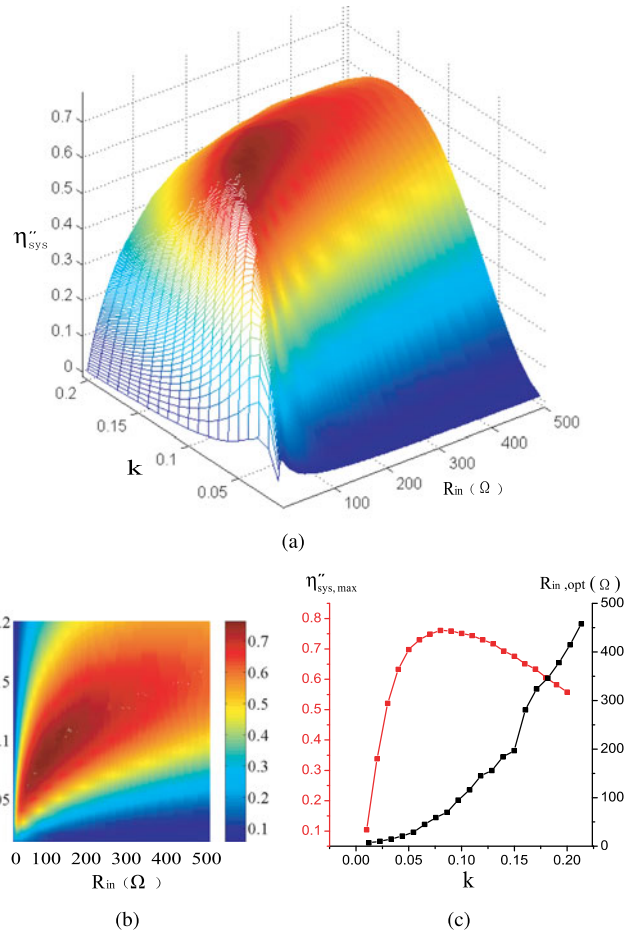

Fig. 8. $\eta''_{\rm sys}$ under different $R_{\rm in}$ and k. (a) 3-D view. (b) 2-D view. (c) Optimal $R_{\rm in}$'s ($R_{\rm in,opt}$).

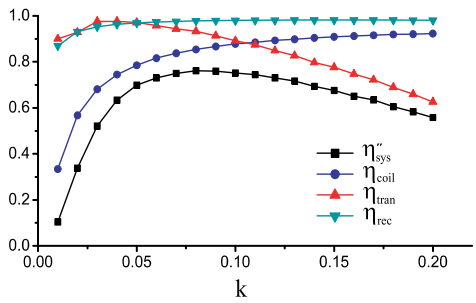

Fig. 9. Maximum efficiencies versus k.

3) maximum $\eta_{\rm tran}$ starts to drop when k is larger than a certain value (about 0.03 here).

Therefore, $\eta''_{\rm sys}$ is significantly influenced by $\eta_{\rm tran}$. In the Smith chart, Fig. 10, the input impedance seen by the PA, $Z_{\rm in}$, is plotted under different $R_{\rm in}$ when $k = 0.01$, 0.1, and 0.2, respectively [also refer to Fig. 6]. The PA source impedance is 50 Ω, i.e., the origin "O" in the Smith chart. The power reflection can be measured by the distance from the points on the curves to the origin [28]. The larger the distance, the smaller the $\eta_{\rm tran}$. For the blue curve ($k = 0.2$), the shortest distance from the points on it

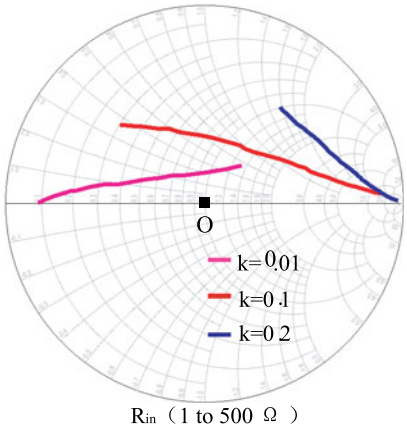

Fig. 10. Smith chart for $Z_{\rm in}$ under different $R_{\rm in}$ when $k = 0.01$, 0.1, and 0.2.

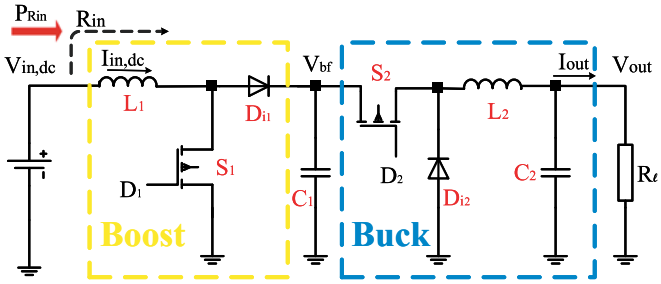

Fig. 11. Cascaded boost-buck converter topology.

to the origin is the longest among the three curves, i.e., a stronger coupling may actually lead to a worse $\eta_{\rm tran}$. This result explains the variations of the maximum $\eta_{\rm tran}$ and thus $\eta''_{\rm sys}$ with an increasing k in Fig. 9. As discussed in the previous section, power reflection can be eliminated with the optimal load $Z_{l,{\rm tran,opt}}$, i.e., a 100% $\eta_{\rm tran}$ [see (13)]. However, when the rectifier is added, the nonlinear behavior of the diodes makes it difficult to realize an optimal Z_l. Because the parasitic parameters of the diodes, especially the junction capacitance, become significant at megahertz, they will introduce the imaginary part to the actual Z_l, and thus make the impedance matching difficult by only adjusting $R_{\rm in}$. Theoretically, an impedance matching network can be inserted between circuits to minimize the power reflection. Thus, the usual experience is still correct that a stronger coupling of the coils leads to a higher system efficiency. However, as mentioned in Section I the impedance matching network itself may introduce additional power loss, extra space, and weight to the system. Besides, in a dynamic environment, the load may represent a changing impedance over time. This means a fixed design of impedance matching network may not function at its designed performance. In the following section, a boost-buck converter is used to provide an equivalent optimal load resistance, i.e., $R_{\rm in,opt}$ seen by the rectifier. The dc–dc converter is controlled to track the optimal load resistances in a dynamic environment such as with changing of relative position between coils and load characteristics over time, and thus maintaining a high overall system efficiency. The tracking scheme can also alleviate the need of a tunable impedance matching network.

III. Tracking of Optimal Load

A. Cascaded Boost-Buck Converter

DC–DC converters can be utilized to control equivalent load resistance $R_{\rm in}$ seen by the rectifier. In [27], six basic dc–dc converter topologies, buck, boost, buck-boost, Ćuk, single-ended primary-inductor converter (SEPIC), and Zeta converters, are first reviewed; then, a new cascaded boost-buck dc–dc converter is proposed to provide an optimal equivalent load resistance through static control. In this paper, dynamic control (i.e., tracking) of the dc–dc converter is discussed based on the above efficiencies analysis. This feedback-based control enables the tracking of the optimal load resistance $R_{\rm in,opt}$ in a dynamic environment, where there are variations in relative position of coils Δk and load characteristics ΔR_l, etc. [see Figs. 6 and 8(c)].

The topology of the cascaded boost-buck converter is shown in Fig. 11. Here, $V_{\rm in,dc}$, $V_{\rm out}$, $I_{\rm in,dc}$ and $I_{\rm out}$ are the input and output voltages and currents of the dc–dc converter, respectively. V_{bf} is buffer capacitor C_1 voltage. D_1 and D_2 are the duty cycles of the switches S_1 and S_2, respectively. In the buck mode (S_1 OFF), assuming there is no power loss, then

$$\frac{V_{\rm in,dc}^2}{R_{\rm in}} = \frac{V_{\rm out}^2}{R_l}. \tag{20}$$

Since

$$V_{\rm out} = D_2 V_{bf} \text{ and } V_{bf} = V_{\rm in,dc} \tag{21}$$

then

$$R_{\rm in} = \frac{R_l}{D_2^2}. \tag{22}$$

Since the duty cycle D_2 can be controlled between 0 and 1, the range of the equivalent load resistance $R_{\rm in}$ is from R_l to $+\infty$. Similarly, in the boost mode (S_2 ON), its input resistance is

$$R_{\rm in} = (1 - D_1)^2 R_l \tag{23}$$

namely a $R_{\rm in}$ from 0 to R_l. Thus, the cascaded connection of the boost and buck converters provides a general solution to match the equivalent load resistant to any specific value from 0 Ω to $+\infty$, while the conventional "single-switch" buck-boost converter is inconvenient due to its opposite polarity between input and output. The behavior of the cascaded converter is also convenient to control and predict because the boost and buck converters can be separately analyzed. Compared with the conventional "single-switch" topologies, this boost-buck "two-switch" topology is attractive here due to its easiness in analysis, control, and implementation. In real applications, if the ranges of variation in the real load and relative position of coils are preknown, it is possible to apply the "single-switch" buck or boost converter, thus further improve the overall system efficiency.

For the cascaded dc–dc converter,

$$V_{bf} = \frac{1}{1 - D_1} V_{\rm in,dc} \tag{24}$$

TABLE II
PARAMETERS OF THE CASCADED BOOST-BUCK CONVERTER

S_1, S_2	IFR540N (IR)
D_{i1}, D_{i2}	BYV29 (NXP)
L_1	4 mH
L_2	1 mH
C_1	3‖470 uF
C_2	470 uF

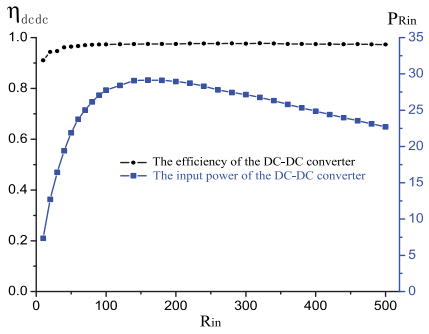

Fig. 12. Efficiency analysis of the cascaded boost-buck dc–dc converter when $k = 0.12$.

and

$$V_{\text{out}} = D_2 V_{bf}. \tag{25}$$

Again assuming zero power loss, from (20), the equivalent load resistance can be derived as

$$R_{\text{in}} = \left(\frac{1 - D_1}{D_2}\right)^2 R_l. \tag{26}$$

Here, a new control parameter D is defined as

$$D = D_1 + D_2. \tag{27}$$

Therefore, in the buck mode

$$D_1 = 0 \text{ and } D = D_2 \tag{28}$$

and in the boost mode

$$D_2 = 1 \text{ and } D = 1 + D_1. \tag{29}$$

By controlling D between 0 and 2, the two modes can be smoothly switched. For a fixed R_l, the larger D, the smaller the equivalent load resistance R_{in}.

Here, the efficiency of the cascaded boost-buck dc–dc converter is analyzed using PSIM, an electronic circuit simulation software package developed by Powersim. This is because that ADS cannot analyze the time-domain behavior of the dc–dc converter with the S-parameters. However, the dc–dc converter should be analyzed as a subsystem in the entire megahertz WPT system. The solution is to record the output power of the rectifier in ADS and use the data as the input for the dc–dc converter in PSIM. Table II lists the parameters of the cascaded boost-buck dc–dc converter in the simulation [see Fig. 11]. This dc–dc converter is used in the final experimental system. Fig. 12 shows the efficiency and input power of the dc–dc converter versus R_{in} when $k = 0.12$. The input power is proportional to the system efficiency η''_{sys} as discussed in Section II-C. Again, the input power is maximized when R_{in} reaches its optimal value $R_{\text{in,opt}}$. High efficiency of the dc–dc converter, about 95%, is maintained in a wide range of R_{in}. Thus, adding the cascaded dc–dc converter does not significantly affect the value of $R_{\text{in,opt}}$ and the overall efficiency of the final system.

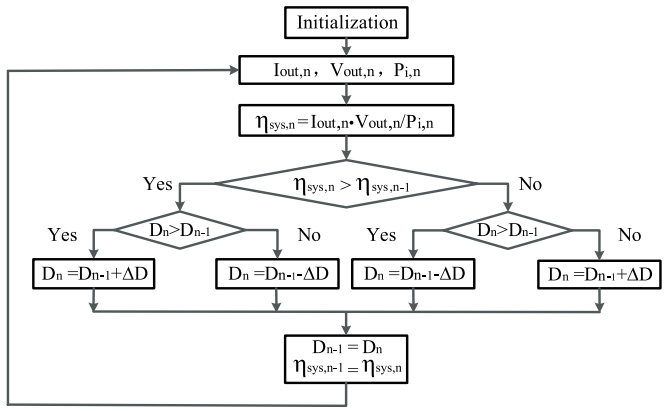

Fig. 13. Flowchart of the P&O-based tracking.

B. P&O-Based Tracking

As shown in Figs. 7 and 8, for a specific mutual-inductance coefficient k, there is a single load resistance R_{in} that enables the maximum system efficiency. In a real WPT system, various variations exist such as in relative position of coils and load characteristics. Tracking of the optimal load resistance is important to ensure a high overall efficiency of the WPT system. Similar consideration can be found in the well-known maximum power point tracking (MPPT) technique, which is widely applied in photovoltaic systems [29]. Unlike MPPT, here the purpose of the tracking is to maximize the overall system efficiency, and the target is determined through a system-level approach, i.e., based on the interactions among subsystems both before and after the dc–dc converter.

In order to verify the tracking of the optimal load resistance, a simple perturbation and observation (P&O) method is implemented in the following experiments [29]. Its flowchart is shown in Fig. 13, where n is the newest sampling instant, $V_{\text{out},n}$ and $I_{\text{out},n}$ are the sampled load voltage and current, respectively, $P_{i,n}$ is the sampled incident power from PA. System efficiency $\eta_{\text{sys},n}$ is defined in (1). D is the control parameter that adjusts the equivalent load resistance seen by the rectifier, i.e., R_{in}. A small and constant perturbation ΔD is applied in a step-by-step manner in order to change the equivalent load resistance. Following each perturbation, the system efficiency variation $\Delta\eta_{\text{sys}}(=\eta_{\text{sys},n}\text{-}\eta_{\text{sys},n-1})$ is measured. If $\Delta\eta_{\text{sys}}$ is positive, the adjusted equivalent load resistance approaches its optimal value, and thus a perturbation with a same sign needs to be applied in the following stage. On the contrary, a negative $\Delta\eta_{\text{sys}}$ indicates that the current equivalent load resistance deviates from the optimal value, and a perturbation with an opposite sign has to be applied. This procedure is iteratively repeated

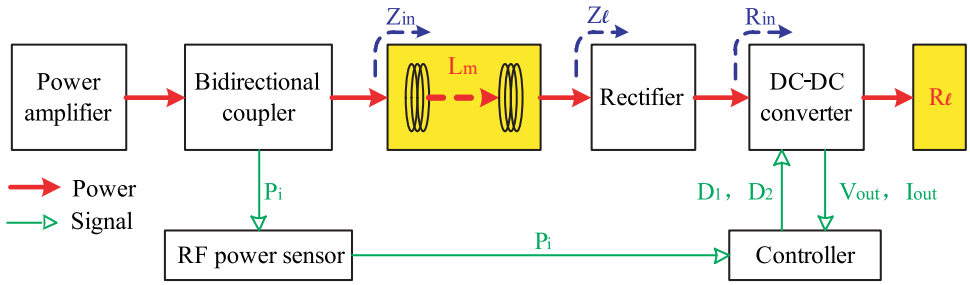

Fig. 14. System configuration for the tracking of the optimal load.

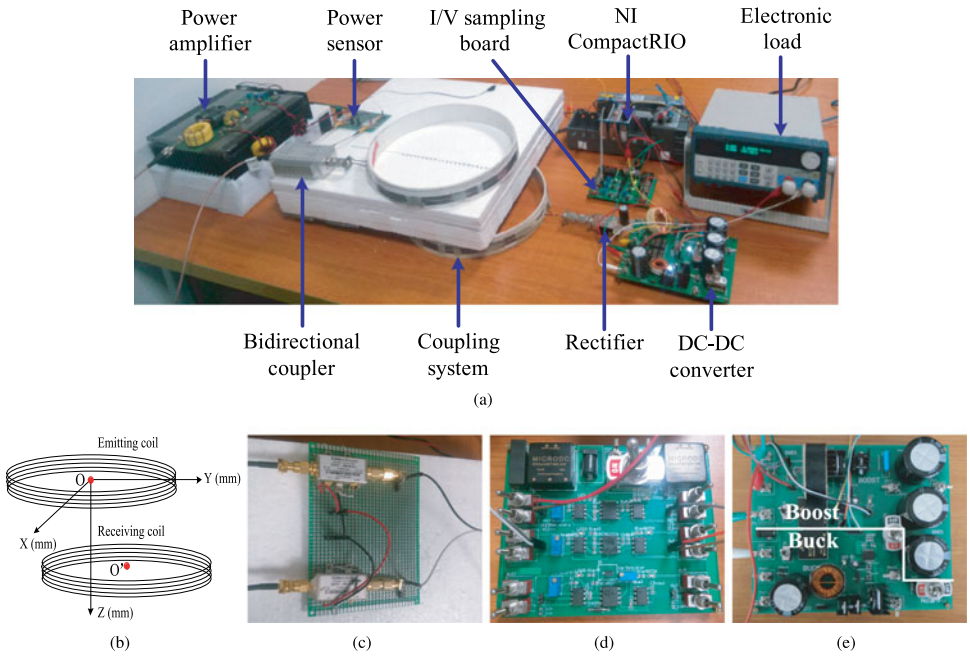

Fig. 15. Experimental WPT system. (a) Overall system. (b) Relative position of coils. (c) Power sensor. (d) *I/V* sampling board. (e) Cascaded dc–dc converter.

until the optimal load resistance is reached. In this P&O-based tracking, three feedback signals are needed, the voltage and current of the load ($V_{\rm out}$ and $I_{\rm out}$) and the incident power from PA (P_i).

C. System Implementation

The system configuration for the tracking of the optimal load is shown in Fig. 14. In the system, the bidirectional coupler provides a signal sample for the measurement of the incident power P_i from PA. This signal is detected by the power sensor and converted to an analog signal. The controller receives the three feedback signals, P_i, $V_{\rm out}$, and $I_{\rm out}$, and implements the P&O-based tracking. Finally, D_1 and D_2, the duty cycles for the boost-buck dc/dc converter, are determined based on the control parameter D [see (28), (29)].

The final experimental WPT system is illustrated in Fig. 15, which consists of a 13.56-MHz class-D PA, a power sensor (Mini-Circuits ZX47-40LN-S+) for the sensing of the incident power P_i, two resonance coils, a rectifier using SiC Schottky diodes, a cascaded boost-buck dc–dc converter, a NI CompactRIO-based data acquisition (DAQ) and control system, and an electronic load. The incident power from PA (P_i) is measured by the power sensor and feedbacked to the DAQ system. The voltage and current of the load ($V_{\rm out}$ and $I_{\rm out}$) are sampled through an *I/V* sampling board. The P&O-based tracking control and the following duty cycle control of the dc–dc converter are both implemented using the NI CompactRIO embedded control system. Besides the *I/V* sampling board, the cascaded dc–dc converter is also designed and fabricated in house. The switching frequency of the dc–dc converter is 20 kHz, and its dimension is 220 mm×160 mm.

IV. Experimental Results

In the following experiments, 40-W incident power from the 13.56-MHz PA is chosen to demonstrate a medium power transfer capability. The coupling system is composed of two identical

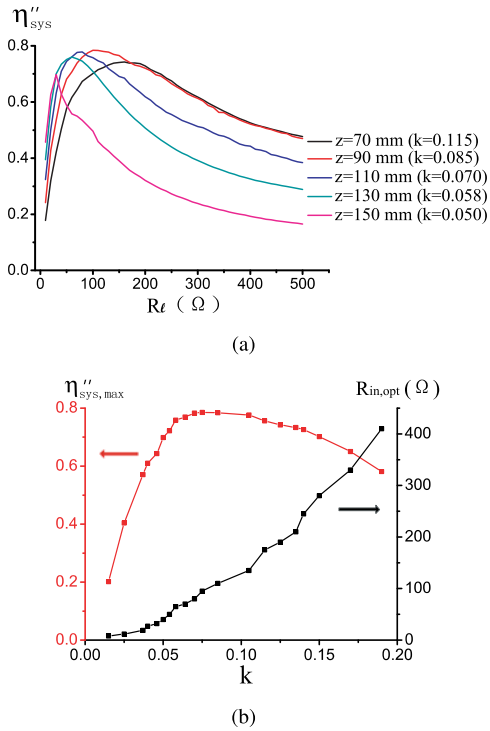

Fig. 16. System static characteristics. (a) System efficiency versus different coil distance z and $R_{\rm in}$. (b) Maximum system efficiency and optimal load resistance versus k.

five-turn helical coils with a diameter of 320 mm. The relative position of coils is illustrated in Fig. 15(b). O and O' are the centers of the emitting and receiving coils, respectively. In 3-D coordinates, the center of the emitting coil O is the origin of the coordinates, i.e., (0, 0, 0). The x, y, z are distances between the centers, O and O', of the two coils in x, y, and z directions, respectively. In the experiments, the relative position of the coils is represented by the location of O' (the center of the receiving coil) in its 3-D coordinates, (x, y, z).

A. Static Characteristics

First, the electronic load is directly connected with the rectifier. The cascaded dc–dc converter is not included in this case. The static characteristics of the real experimental WPT system is measured in order to validate the previous analysis on the system efficiency. O and O' are aligned and the receiving coil moves along the z-axis. Under a specific distance between coils z, the relationship between system efficiency $\eta_{\rm sys}$ and $R_{\rm in}$, the load resistance after the rectifier, is shown in Fig. 16(a). $R_{\rm in}$ is tuned using the electronic load. The maximum system efficiency and the optimal load resistance versus the mutual-inductance coefficient k are plotted in Fig. 16(b). This experimental result is consistent with the previous analysis [see Fig. 8(c)].

B. Variation in Load Resistance

In this experiment, O' is fixed at (0, 0, 100), i.e., a constant k [see Fig. 15(b)]. The cascaded boost-buck converter is controlled to implement the P&O-based tracking of the optimal load. The

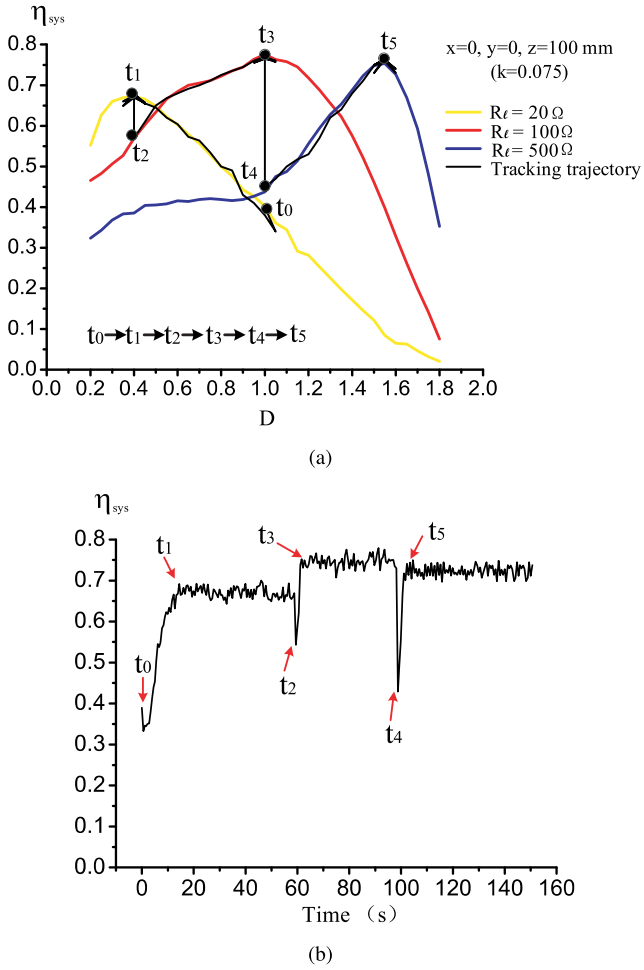

Fig. 17. Tracking of optimal load resistances with a varying R_l. (a) Tracking trajectory. (b) Time response.

initial D is 1, and the perturbation ΔD is selected as 0.05. The system efficiency $\eta_{\rm sys}$ curves versus D for three load resistances (R_l), 20, 100, and 500 Ω, are measured in steady state and shown in Fig. 17(a) with different colors. Those data are calculated and recorded using the NI compact-RIO-based DAQ and control system. The experiment starts from time t_0 with 20-Ω load resistance. The optimal load resistance under the constant k is reached at t_1 by the feedback-based control of the parameter D [see (22), (23), (27)–(29)]. At time t_2, the load resistance R_l is switched from 20 to 100 Ω. Since the equivalent load resistance seen by the rectifier deviates from its optimal value, a quick drop of the system efficiency is observed. Through the tracking control using the cascaded dc–dc converter (i.e., the adjustment of D), the optimal load resistance is reached again at t_3, thus a high system efficiency is achieved, which is consistent with the previous theoretical analysis. A similar procedure is repeated at t_4 and t_5, when the load resistance is changed from 100 to 500 Ω [refer to the tracking trajectory in black]. Besides the tracking trajectories, the waveforms at the changing points are also shown in Fig. 17(b). It can be seen that the optimal load resistance under the constant k is successfully tracked at t_1, t_3,

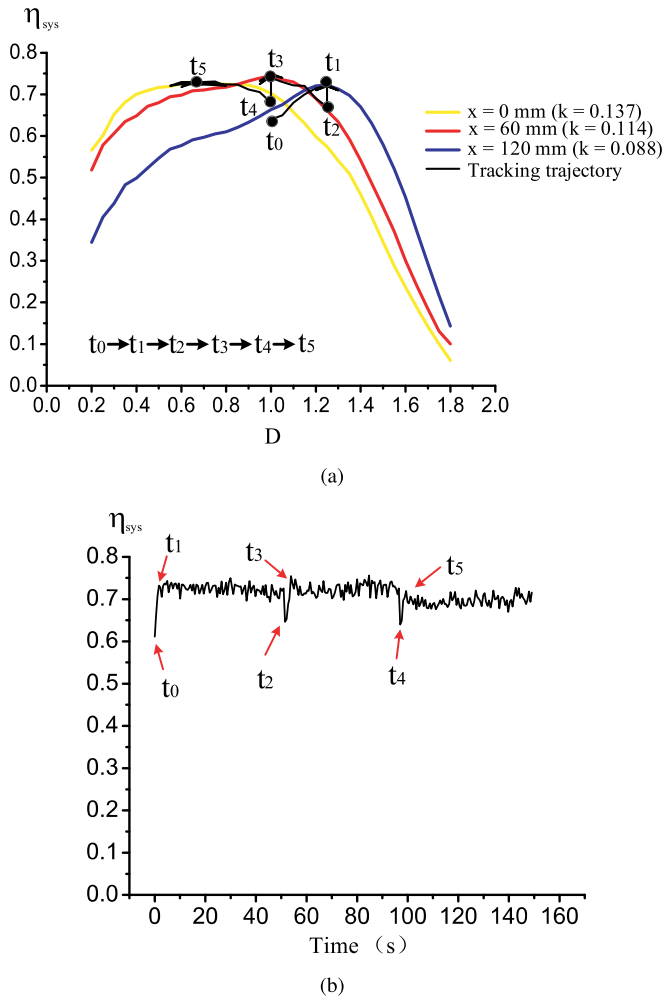

Fig. 18. Tracking of optimal load resistances with a varying k. (a) Tracking trajectory. (b) Time response.

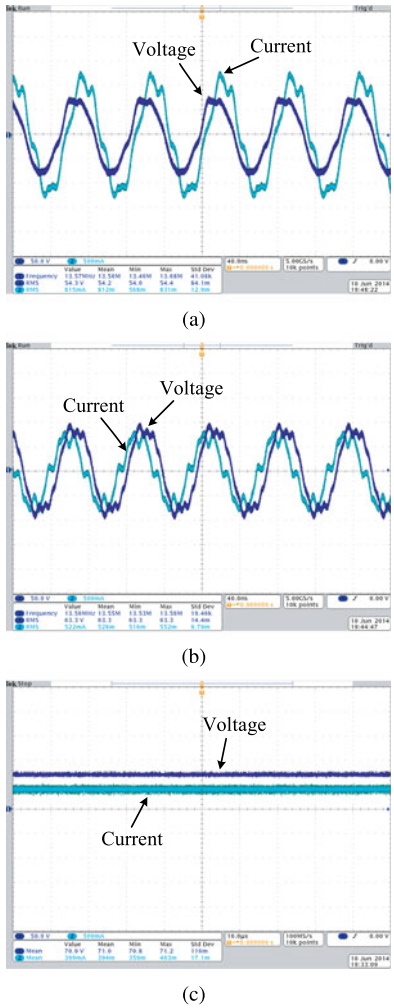

Fig. 19. Example waveforms for input voltages and currents in the megahertz WPT system ($O^{'}$ =(0,0,70) and $R_l = 100\,\Omega$). (a) Coupling system. (b) Rectifier. (c) Cascaded dc–dc converter.

and t_5 for the three real load resistances, 20, 100, and 500 Ω, respectively.

C. Variation in Relative Position of Coils

This experiment demonstrates the tracking under a constant load resistance, R_l (=100 Ω) and a varying relative position of coils, i.e., variation in k. The initial position of $O^{'}$ is (120, 0, 70) [see Fig. 15(b)]. Fig. 18(a) shows the three colorful efficiency curves versus D for three positions, $x = 0$, 60, and 120 mm with fixed y (= 0 mm) and z (= 70 mm), which again are measured in steady state. The waveforms at the changing points are shown in Fig. 18(b). The relative position is adjusted from $x = 120$ mm to $x = 60$ mm at t_2, and then from $x = 60$ to $x = 0$ at t_4. Again at t_2, a quick drop of the system efficiency is observed because the equivalent load resistance seen by the rectifier deviates from its optimal value due to the variation of k. Through the P&O-based tracking control (i.e., the adjustment of D), the optimal load resistance under the newest k is reached at t_3 that corresponds to the position of $x = 60$ mm. A similar procedure is repeated at t_4 and t_5, when x is changed again from 60 to 0 mm [refer to the tracking trajectory in black]. As shown in Fig. 18(a) and (b), the various optimal load resistances are reached at t_1, t_3, and t_5, after the variation occurs in the relative position of coils, and thus k.

D. Operating Waveforms and Discussions

Fig. 19 shows the example waveforms for the coupling system, the rectifier, and the cascaded dc–dc converter when the megahertz WPT system is in its steady-state operation. Here, $O^{'}$ is (0, 0, 70) and R_l is 100 Ω, namely the state at t_5 in Fig. 18. As shown in Fig. 19(a), harmonic waves exist in the input voltage and current of the coupling system. This is because it is standard to tune RF power amplifiers for matching a 50 Ω load, but the matching of the optimal load (i.e., R_{in}) alone is not able to fully meet this requirement, i.e., a 50 Ω load seen by the RF PA. As discussed in Section II-C, although theoretically an impedance matching network could be inserted, the network itself will introduce additional power loss, extra space, and weight. Especially, it is complicated to design a tunable impedance matching

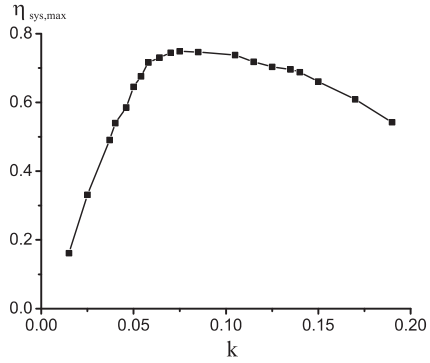

Fig. 20. Overall system efficiency under different k.

network when the load is changing over time [26]. As shown in the above experimental results, the tracking of the optimal load using the cascaded dc–dc converter minimizes the effect of a dynamic load to the system efficiency. It also alleviates the requirements on the impedance network. Besides, for the coupling system, its input current lags behind its input voltage, namely an inductive $Z_{\rm in}$. This is consistent with the previous analysis using the Smith chart in Fig. 10. In the Smith chart, the upper half circle corresponds to inductive impedances.

Fig. 19(b) shows the input voltage and current for the rectifier. There is relatively large harmonic distortion due to the nonlinear behavior of the diodes at megahertz. The waveforms are quite different with those of rectifiers working at frequencies in conventional power electronics (kilohertz or lower). It is known that at high frequencies, the parasitic capacitance of diodes becomes obvious. Thus, they cannot be treated as an ideal passive switch anymore. Because of the different nature of the megahertz WPT systems, it is important to analyze the impedance matching based on the transmission line theory [28]. The input voltage and current of the dc–dc converter are shown in Fig. 19(c). The equivalent $R_{\rm in}$ (about 180 Ω) can be directly calculated, and its value 180 Ω is consistent with the optimal load resistance for $z = 70$ mm in Fig. 16(a) [see the black curve].

Finally, Fig. 20 gives the overall maximum system efficiency $\eta_{\rm sys,max}$ under different mutual inductance coefficient k when $R_l = 100\ \Omega$ [see (2)]. Its basic trend is similar to that of $\eta''_{\rm sys}$ in Fig. 16(b), where the dc–dc converter is not included. This verifies the limited influence of the dc–dc converter on the overall system performance.

V. Conclusion

In this paper, a detailed analysis is carried out on the efficiencies of a WPT system at both circuit and system levels. It is derived and experimentally verified that under a specific mutual inductance between the emitting and receiving coils, there exists an optimal load resistance for a high system efficiency. The tracking system for the optimal load is then developed using the P&O-base algorithm and hardware such as the cascaded boost-buck dc–dc converter, efficiency sensing system, and a controller. A 13.56-MHz WPT system is demonstrated experimentally to validate the efficiency analysis and the feedback-based tracking control. At a power level of 40 W, the overall system efficiency from the source to the final load is maintained about 70% under various load resistances and relative positions of coils. Future direction of this paper is to extend the analysis and control into a multireceiver WPT system, in which an optimized power distribution among the multiple receiving coils need be studied.

References

[1] N. Tesla, "The transmission of electric energy without wires, " in *The Electrical World and Engineer*. New York, NY, USA: McGraw-Hill, Mar. 5, 1904.

[2] J. Fishelson, K. Heaslip, W. Louisell, and K. Womack, "An evaluation framework for an automated electric transportation network," presented at the *90th Transp. Res. Board Annu. Meet.*, Washington DC, USA, Jan. 2011.

[3] H. Rakouth, J. Absmeier, A. Brown, Jr., I.-S. Suh, R. Sumner, and R. Henderson, "EV charging through wireless power transfer: Analysis of efficiency optimization and technology trends," in *Proc. FISITA World Automotive Congr.*, Beijing, China, Nov. 2013, pp. 871–884.

[4] N. Shinohara, "Power without wires," *IEEE Microw. Mag.*, vol. 12, no. 7, pp. S64–S73, Dec. 2011.

[5] J. T. Howell, M. J. O'Neill, and R. L. Fork, "Advanced receiver/converter experiments for laser wireless power transmission," in *Proc. 4th Int. Conf. Solar Power Space*, vol. 567, Granada, Spain, 30 Jun.–2 Jul. 2004, pp. 187–194.

[6] A. Kurs, A. Karalis, R. Moffatt, J. D. Joannopoulos, P. Fisher, and M. Soljačić, "Wireless power transfer via strongly coupled magnetic resonances," *Science*, vol. 317, no. 5834, pp. 83–86, 2007.

[7] C.-S. Wang, O. H. Stielau, and G. A. Covic, "Design considerations for a contactless electric vehicle battery charger," *IEEE Trans. Ind. Electron.*, vol. 52, no. 5, pp. 1308–1314, Oct. 2005.

[8] A. P. Hu, *Wireless/Contactless Power Supply:-Inductively Coupled Resonant Converter Solutions*. Saarbrucken, Germany: VDM Publishing, 2009.

[9] N. A. Keeling, G. A. Covic, and J. T. Boys, "A unity-power-factor IPT pickup for high-power applications," *IEEE Trans. Ind. Electron.*, vol. 57, no. 2, pp. 744–751, Feb. 2010.

[10] K. Kobayashi, T. Pontefract, Y. Kamiya, and Y. Daisho, "Development and performance evaluation of a non-contact rapid charging inductive power supply system for electric micro-bus," presented at the *7th IEEE Vehicle Power Propulsion Conf.*, Chicago, IL, USA, Sep. 2011.

[11] M. Budhia, G. A. Covic, and J. T. Boys, "Design and optimization of circular magnetic structures for lumped inductive power transfer systems," *IEEE Trans. Power Electron.*, vol. 26, no. 11, pp. 3096–3108, Nov. 2011.

[12] W. Zhang, S.-C. Wong, C. Tse, and Q. Chen, "Design for efficiency optimization and voltage controllability of series–series compensated inductive power transfer systems," *IEEE Trans. Power Electron.*, vol. 29, no. 1, pp. 191–200, Jan. 2014.

[13] T. Imura, H. Okabe, T. Koyanagi, M. Kato, T. Beh, M. Ote, J. Shimamoto, M. Takamiya, and Y. Hori, "Proposal of wireless power transfer via magnetic resonant coupling in kHz-MHz-GHz," presented at the *General Conf. Inst. Electron., Inf. Commun. Engineers*, Sendai, Japan, Mar. 2010.

[14] *Improving the Effectiveness, Flexibility and Availability of Spectrum for Short Range Devices*, Radiocommunication Advisory Group, International Telecommunication Union, Document RAG07-1/17-E, 2007.

[15] S.-H. Lee and R. D. Lorenz, "Development and validation of model for 95%-efficiency 220-W wireless power transfer over a 30-cm air gap," *IEEE Trans. Ind. Appl.*, vol. 47, no. 6, pp. 2495–2504, Nov./Dec. 2011.

[16] S. Hui, W. Zhong, and C. Lee, "A critical review of recent progress in mid-range wireless power transfer," *IEEE Trans. Power Electron.*, vol. 29, no. 9, pp. 4500–4511, Sep. 2014.

[17] D. Krschner and C. Rathge, "Maximizing DC-to-load efficiency for inductive power transfer," *IEEE Trans. Power Electron.*, vol. 28, no. 5, pp. 2437–2447, May 2013.

[18] M. W. Baker and R. Sarpeshkar, "Feedback analysis and design of RF power links for low-power bionic systems," *IEEE Trans. Biomed. Circuits Syst.*, vol. 1, no. 1, pp. 28–38, Mar. 2007.

[19] W. Zhong, X. Liu, and S. R. Hui, "A novel single-layer winding array and receiver coil structure for contactless battery charging systems with free-positioning and localized charging features," *IEEE Trans. Ind. Electron.*, vol. 58, no. 9, pp. 4136–4144, Sep. 2011.

[20] J. J. Casanova, Z. N. Low, and J. Lin, "Design and optimization of a class-e amplifier for a loosely coupled planar wireless power system," *IEEE Trans. Circuits Syst. II: Exp. Briefs*, vol. 56, no. 11, pp. 830–834, Nov. 2009.
[21] Z. N. Low, R. A. Chinga, R. Tseng, and J. Lin, "Design and test of a high-power high-efficiency loosely coupled planar wireless power transfer system," *IEEE Trans. Ind. Electron.*, vol. 56, no. 5, pp. 1801–1812, May 2009.
[22] B. Choi, J. Nho, H. Cha, T. Ahn, and B. Choi, "Design and implementation of low-profile contactless battery charger using planar printed circuit board windings as energy transfer device," *IEEE Trans. Ind. Electron.*, vol. 51, no. 1, pp. 140–147, Feb. 2004.
[23] C.-S. Wang, G. A. Covic, and O. H. Stielau, "Investigating an LCL load resonant inverter for inductive power transfer applications," *IEEE Trans. Power Electron.*, vol. 19, no. 4, pp. 995–1002, Jul. 2004.
[24] A. P. Sample, B. H. Waters, S. T. Wisdom, and J. R. Smith, "Enabling seamless wireless power delivery in dynamic environments," *Proc. IEEE*, vol. 101, no. 6, pp. 1343–1358, Apr. 2013.
[25] T. P. Duong and J.-W. Lee, "Experimental results of high-efficiency resonant coupling wireless power transfer using a variable coupling method," *IEEE Microw. Wireless Compon. Lett.*, vol. 21, no. 8, pp. 442–444, Aug. 2011.
[26] T. C. Beh, M. Kato, T. Imura, S. Oh, and Y. Hori, "Automated impedance matching system for robust wireless power transfer via magnetic resonance coupling," *IEEE Trans. Ind. Electron.*, vol. 60, no. 9, pp. 3689–3698, Sep. 2013.
[27] M. Fu, C. Ma, and X. Zhu, "A cascaded boost-buck converter for high efficiency wireless power transfer systems," *IEEE Trans. Ind. Informat.*, vol. 10, no. 3, pp. 1972–1980, Aug. 2014.
[28] D. M. Pozar, *Microwave Engineering*. Hoboken, NJ, USA: Wiley, 2009.
[29] A. Reza Reisi, M. Hassan Moradi, and S. Jamasb, "Classification and comparison of maximum power point tracking techniques for photovoltaic system: A review," *Renewable Sustainable Energy Rev.*, vol. 19, pp. 433–443, 2013.

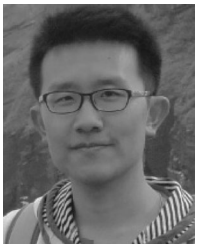

Minfan Fu (S'13) received the B.S. and M.S. degrees both in electrical and computer engineering from the University of Michigan-Shanghai Jiao Tong University Joint Institute, Shanghai Jiao Tong University, Shanghai, China, in 2010 and 2013, respectively, where he is currently working toward the Ph.D. degree.

His research interests include power electronics, control, and their applications in wireless power transfer.

He Yin (S'13) received the B.S. degree in the electrical and computer engineering from University of Michigan-Shanghai Jiao Tong University Joint Institute, Shanghai Jiao Tong University, Shanghai, China, in 2012. He is currently working toward Ph.D. degree.

His research interests include optimization and control of alternative energy systems such as energy storage systems using ultracapacitors and wireless power transfer systems.

Xinen Zhu (S'04–M'09) received the B.Eng. (Hons.) degree in electronic and communication engineering from City University of Hong Kong, Hong Kong, in 2003, and the M.S. and Ph.D. degrees in electrical engineering from The University of Michigan, Ann Arbor, MI, USA, in 2005 and 2009, respectively.

He is currently a tenure-track Assistant Professor of electrical and computer engineering with the University of Michigan-Shanghai Jiao Tong University Joint Institute, Shanghai Jiao Tong University, Shanghai, China. His research interests include wireless power transfer, tunable RF/microwave circuits, and ferroelectric thin films.

Chengbin Ma (M'05) received the B.S.E.E. (Hons.) degree from East China University of Science and Technology, Shanghai, China, in 1997, and the M.S. and Ph.D. degrees both in the electrical engineering from University of Tokyo, Tokyo, Japan, in 2001 and 2004, respectively.

He is currently a tenure-track Assistant Professor of electrical and computer engineering with the University of Michigan-Shanghai Jiao Tong University Joint Institute, Shanghai Jiao Tong University, Shanghai, China. He is also with a joint faculty appointment in the School of Mechanical Engineering, Shanghai Jiao Tong University. Between 2006 and 2008, he held a Postdoctoral position with the Department of Mechanical and Aeronautical Engineering, University of California Davis, CA, USA. From 2004 to 2006, he was a R&D Researcher with Servo Laboratory, Fanuc Limited, Yamanashi, Japan. His research interests include wireless power transfer, networked hybrid energy systems, and mechatronic control.